# DIG: Discrete Iso-contour Geodesics
# for Topological Analysis of Voxelized Objects

Gurman Bhalla and Partha Bhowmick[✉]

Department of Computer Science and Engineering,
Indian Institute of Technology, Kharagpur, India
gurman.bhalla@gmail.com, bhowmick@gmail.com

**Abstract.** Discretized volumes and surfaces—used today in many areas of science and engineering—are approximated from the real objects in a particular theoretical framework. After a discretization produces a triangle mesh (2-manifold surface), a well-formed voxel set can be prepared from the mesh by voxelization of its constituent triangles based on some digitization principle. Since there exist different topological models of digital plane, choosing the appropriate model to meet the desired requirement appears to be of paramount importance. We introduce here the concept of discrete iso-contour geodesics (DIG) and show how they can be constructed on a voxelized surface with the assurance of certain topological requirements, when the voxelization conforms to the naive model with judicious inclusion of Steiner voxels from the graceful model, as and when needed. We also show some preliminary results on its practical application towards extraction of high-level topological features of 3D objects, which can subsequently be used for various shape-analytic applications.

**Keywords:** Digital geometry · Discrete topology · Iso-contour geodesics · Shape analysis · Voxelization

## 1 Introduction

Voxelization today is not only important in the field of object discretization and representation but also gaining remarkable progress in additive manufacturing through rapid prototyping (RP) techniques like stereo-lithography, 3D printing, and fused deposition modeling [11,19–21,30]. Hence, the collection of work related to voxelization, as seen in today's literature, can be divided into two categories—one covering the theories and algorithmic solutions for object discretization and another dealing with different RP techniques using digital technology. The latter category mostly relies on a *digital building matter* in the sense that the building block is a digital unit or *voxel*, as opposed to the analog (continuous) material used in conventional RP [6,17,18,28,32].

Whether the subject relates to analytical discretization or relates to physical manufacturing, the underlying theory or methodology of voxelization has a strong impact on the consistency or on the solidity of the resultant product.

In either case, these characteristics can be analyzed well in the purview of discrete geometry and topology, as a collection of voxels is usually obtained by a particular process in a certain theoretical framework [23,27]. In our work, we focus on this with a two-fold objective—first to show how a surface should be voxelized for its readiness to discrete iso-contour geodesic (DIG) construction and then to demonstrate the usefulness of DIG in extraction of high-level topological information from a voxelized object.

## 1.1    Existing Work

We give here a brief review of the development and the state-of-the art practices related to voxelization and also to computation of discrete geodesics and iso-contours.

**Voxelization.** The early work on physical modeling of a surface or volume element can be seen in [19,30,31] and in the articles referred to therein. Those work, however, did not address the topological issues related to voxelization. The theoretical frameworks along with the topological issues came up gradually in a later stage. For example, in [9], some of the topological properties were discussed, which included holes, cavities, simple points, separability, and penetration.

With the growing need for digitization and cutting-edge technology, different techniques for voxelization have been proposed off and on, taking into account different apparatus, computational models, cost factors, and product requirement. A low-cost methodology based on z-buffer and multi-view depth information is developed in [22]. To incorporate an anti-aliasing effect during voxel rendition, a multi-resolution technique is proposed in [10]. For adding more features available in graphics workstations, such as texture mapping and frame-buffer blending functions, a hardware-accelerated approach is shown to be effective in [16]. The idea of exploiting programmable graphics hardware is also used in [13] for voxelization of a polygonal model after mapping it into three sheet buffers and then synthesizing into a single worksheet recording the volumetric representation of the target.

Voxelization is also useful for simplification and repair of a polygonal model, as shown in [29], with 3D morphological operations on the scan-converted voxel set. Further, with the emergence of GPU functionalities, a variety of applications with voxelized objects have come up in recent time. For example, in [24], a GPU-accelerated approach is proposed for creation of multi-valued solid volumetric models with different solid slice functions and material description in order to make it useful for different applications like collision detection, medical simulation, volume deformation, 3D printing, and computer art. In [15], a filtering algorithm is designed to build a density estimate for deduction of normals from the voxelized model, which is shown to be useful in simulation of translucency effects and particle interactions. In fact, very recently, many such real-time simulations and applications are shown to be efficiently realizable when a voxelized dataset is used; these include urban modeling [34], octree-based sparse voxelization for 3D animation [12], fluid simulation with dynamic obstacles [38], discrete radiosity [25], light refraction and transmittance in complex scenes [7], etc.

**Geodesics.** The literature on geodesics and iso-contours, as on today, is predominantly focused on closed orientable 2-manifold surfaces, i.e., objects with triangulated-mesh representation in the Euclidean space. Hence, the techniques are mostly from differential and computational geometry; see, for example, [1,8,26,33,35–37]. As geodesics find various applications in remeshing, non-rigid registration, surface parametrization, shape editing and segmentation, the notion of approximate geodesic distance is also proposed recently in [36] as a practical alternative for the exact solution [35].

In the domain of voxel complexes, however, no significant work can be found on discrete geodesics, barring a few [8,12]. In [8], the concept of visibility—a well-known concept in computational geometry—is defined in the discrete space based on digital straightness. In [12], as sparse (i.e., highly disconnected) voxel set is used, the geodesic metric is based on Euclidean norm.

### 1.2   Our Contribution

As briefed in Sect. 1.1, a multitude of work have been carried out on voxelization of 2-manifolds and on geodesics in the Euclidean space. However, geodesics on voxelized (i.e., 3-manifold) surfaces and their topological properties have not been studied so far. This motivates us to look into this interesting problem. We introduce here the concept of *discrete iso-contour geodesics* (DIG) that can be constructed on a well-formed voxelized surface and then demonstrate their usefulness in shape-analytic applications similar to those in the Euclidean domain.

Henceforth in this paper, a voxelized curve (DIG in our case) or a voxelized surface means discrete approximation of its real counterpart by a set of voxels in a certain topological model. In order to ensure that the concerned object is well-defined in the voxelized space, the connectivity and related topological issues come up alongside, which are addressed and fixed in this paper.

## 2   Voxelization of 2-Manifolds

We discuss here some definitions and concepts related to topology of voxel complexes and the underlying metric space, which are relevant to our work, following the convention as in [23]. For easy understanding and for easily relating the theoretical results with the experimental results on voxelized objects, we discuss the topological concepts in terms of voxels and relations among them, which can be equivalently represented and explained in graph-theoretic terms as well [23,27].

### 2.1   Voxel Topology and Metric Space

A *voxel* is a 3-cell, i.e., an axis-parallel cube-shaped 3-manifold of unit length. Two voxels are said to be 0-, 1-, or 2-*adjacent* if they share a vertex (0-cell), an edge (1-cell), or a face (2-cell), respectively (also called 26-, 18-, 6-neighborhoods [9]). Note that 0-adjacent (1-adjacent) voxels are not treated as adjacent while considering 1-adjacency (2-adjacency).

A voxelized object $A$ means a set of voxels. A $k$-*path* $(k = 0, 1, 2)$ in $A$ is a sequence of voxels from $A$ such that every two consecutive voxels are $k$-adjacent. If a $k$-path exists between every two voxels of $A$, then $A$ is said to be $k$-*connected*. A $k$-*component* is a maximal $k$-connected subset of $A$.

A subset $A'$ of $A$ is $k$-*separating* (w.r.t. $A$) if $A \smallsetminus A'$ is not $k$-connected. In addition, if $A \smallsetminus A'$ has exactly two $k$-components and $A'$ has a voxel $v$ such that $A' \smallsetminus \{v\}$ is still $k$-separating, then $v$ is called a *simple voxel* in $A'$. If now $A'$ contains no simple voxel, then $A'$ is $k$-*minimal* and so has no *tunnel*; and if $A'$ has any tunnel, then it is not 2-separating (see [3] for further details).

The *supercover* $K(X)$ of a set $X \subseteq \mathbb{R}^3$ is the set of all voxels intersected by $X$. The *standard* and the *naive* voxelizations of $X$ are 0- and 1-minimal subsets of $K(X)$. If $X$ is a real plane or its part (such as a triangle in our work), then its naive set $N(X)$ is *functional* in at least one coordinate plane and hence has one-to-one correspondence with its projection on that coordinate plane. For example, if $xy$-plane is functional for $X$, then $N(X)$ has one-to-one correspondence with its projection on the $xy$-plane. Some examples are given in Fig. 1.



(a) Naive                    (b) Standard                    (c) Graceful
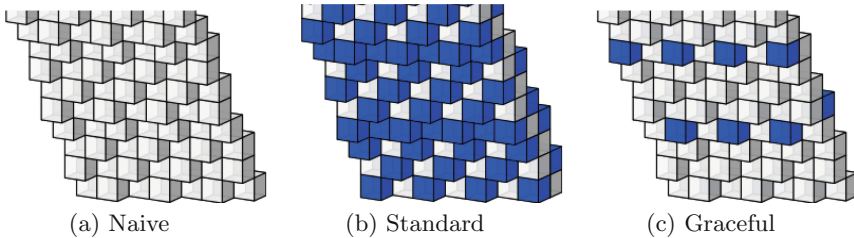
**Fig. 1.** Instances of three models of digital plane for $(a, b, c) = (4, -5, 8)$, in the domain $x \in [-3, 3], y \in [-7, 7]$. White voxels belong to the naive plane and the blue belong to (b) standard or (c) graceful. Notice that the $xy$-plane is functional here only for the naive plane. (Color figure online)

We define $x$-, $y$-, and $z$-*distance* between two (real or integer) points, $p$ and $p'$, as $d_x(p, p') = |i - i'|$, $d_y(p, p') = |j - j'|$, and $d_z(p, p') = |k - k'|$, respectively, where $d_z$ is not applicable in 2D, $p = (i, j)$ and $p' = (i', j')$ in 2D, and $p = (i, j, k)$ and $p' = (i', j', k')$ in 3D. The $x$-distance between $p(i, j, k)$ and a curve/surface $X$ is $d_x(p, X) = d_x(p, p')$ if $\exists\, p'(x', y', z') \in X$ such that $(y', z') = (j, k)$; otherwise, $d_x(p, X) = \infty$. The distances $d_y(p, X)$ and $d_z(p, X)$ are defined in a similar way. Let $D$ denote the set $\{d_x(\cdot), d_y(\cdot)\}$ in 2D and $\{d_x(\cdot), d_y(\cdot), d_z(\cdot)\}$ in 3D. Then the *isothetic distance* between two points $p$ and $p'$ is the *Minkowski norm*, $d_\infty(p, p') = \max\{\delta : \delta \in D\}$, and that between $p$ and a curve/surface $X$ is $d_\perp(p, X) = \min\{\delta : \delta \in D\}$.

As shown in [2], each voxel of a naive plane (triangle in our case) has an isothetic distance of at most $\frac{1}{2}$ from the corresponding real plane. Hence, the naive voxelization results in the best possible approximation of a manifold with the guarantee of one-to-correspondence with the projection (pixel set) on its functional plane.

## 2.2   Homeomorphism of Voxels and 2-Manifolds

Let $S$ be a closed and orientable (2-manifold) surface in the 3D Euclidean space, such that exactly two 2-manifolds (triangles) are incident on each of its 1-manifolds (edges) and at least three 1-manifolds are incident on each of its 0-manifolds (vertices). To derive a 3-manifold representation (naive voxelization) of $S$ in $\mathbb{Z}^3$, we choose a *scale factor* $\xi > 0$ and apply an isotropic scaling on the 0-manifolds of $S$. Next, for every 2-manifold $t \in S$, we make its naive voxelization to obtain $N(t, \xi)$, and hence obtain the naive voxelization of $S$ (scaled by the factor $\xi$) as $N(S, \xi) = \bigcup_{t \in S} N(t, \xi)$. Being closed and orientable, $S$ is a compact surface without any boundary and the outward normal to each 2-manifold $t \in S$ is uniquely determinable, whence the functional plane(s) of each $N(t, \xi)$ is also fixed.

  To define the topological space for $S$, let $v$ be a voxel in $N(S, \xi)$. Then $v$ is obtained in the naive voxelization of one or more 2-manifolds in $S$. So, we define $T(v) = \{t : t \in S \wedge v \in N(t, \xi)\}$ and $\mathcal{S} = \{T(v) : v \in N(S, \xi)\}$. If $\varGamma_\mathcal{S}$ denotes the topology defined on $\mathcal{S}$, then the corresponding topological space becomes $(\mathcal{S}, \varGamma_\mathcal{S})$. Now, to obtain the topological space $(\mathcal{V}, \varGamma_\mathcal{V})$ for $N(S, \xi)$, we define $\mathcal{V} = \{V(v) : v \in N(S, \xi)\}$, where $V(v) = N(T(v), \xi) := \bigcup_{t \in T(v)} N(t, \xi)$. Henceforth, for brevity, we denote $(\mathcal{S}, \varGamma_\mathcal{S})$ and $(\mathcal{V}, \varGamma_\mathcal{V})$ simply by $\mathcal{S}$ and $\mathcal{V}$, respectively [14].

  We show the homeomorphism of $\mathcal{S}$ with $\mathcal{V}$ shortly in Theorem 1. For this, we define a basis $B_\mathcal{S}$ for $\mathcal{S}$ and another $B_\mathcal{V}$ for $\mathcal{V}$, as follows.

(i)   Each $\beta_\mathcal{S}^{(i)} \in B_\mathcal{S}$ contains (as its element) every set $\big\{T(v) : (v \in N(T(v), \xi)) \wedge$ $(x(v) = i)\big\}$, where $x(v)$ denotes the $x$-coordinate of the center of the voxel $v$.
(ii)  If $(\beta_\mathcal{S}^{(i)}, \beta_\mathcal{S}^{(j)}) \in B_\mathcal{S}^2$ and $\beta_\mathcal{S}^{(i)} \cap \beta_\mathcal{S}^{(j)} \neq \emptyset$, then $\beta_\mathcal{S}^{(i)} \cap \beta_\mathcal{S}^{(j)} \in B_\mathcal{S}$.
(iii) Each $\beta_\mathcal{V}^{(i)} \in B_\mathcal{V}$ contains every set $\{V(v) : x(v) = i\}$.
(iv)  If $(\beta_\mathcal{V}^{(i)}, \beta_\mathcal{V}^{(j)}) \in B_\mathcal{V}^2$ and $\beta_\mathcal{V}^{(i)} \cap \beta_\mathcal{V}^{(j)} \neq \emptyset$, then $\beta_\mathcal{V}^{(i)} \cap \beta_\mathcal{V}^{(j)} \in B_\mathcal{V}$.

**Theorem 1.** *The topological spaces $\mathcal{S}$ and $\mathcal{V}$ are homeomorphic for a sufficiently large value of $\xi$.*

*Proof.* Let $f : \mathcal{S} \rightarrow \mathcal{V}$. So, if $T(v), T(v') \in \mathcal{S}$, then $f(T(v)) = V(v) \in \mathcal{V}$ and $f(T(v')) = V(v') \in \mathcal{V}$. As $\xi$ is sufficiently large, $T(v) \neq T(v')$ and $V(v) \neq V(v')$ for any $(v, v')$ with $v \neq v'$. So, $V(v) = V(v') \iff T(v) = T(v') \iff v = v'$, wherefore $f$ is bijective.

  Now, to show that $f$ is continuous, let $v$ be a voxel with $x(v) = i$. Then $T(v)$ belongs to an element of $\beta_\mathcal{S}^{(i)}$, and $f(T(v)) := V(v)$ belongs to an element of $\beta_\mathcal{V}^{(i)}$, which imply $f(\beta_\mathcal{S}^{(i)}) \subset \beta_\mathcal{V}^{(i)}$, or, $\beta_\mathcal{S}^{(i)} \subset f^{-1}(\beta_\mathcal{V}^{(i)})$, whence $f^{-1}(\beta_\mathcal{V}^{(i)})$ is an open set, thus showing $f$ continuous. Similarly, $g := f^{-1} : \mathcal{V} \rightarrow \mathcal{S}$ is also continuous, since $V(v)$ belongs to an element of $\beta_\mathcal{V}^{(i)}$ and $g(V(v))$ to an element of $\beta_\mathcal{S}^{(i)}$, or, $g(\beta_\mathcal{V}^{(i)}) \subset \beta_\mathcal{S}^{(i)}$, or, $\beta_\mathcal{V}^{(i)} \subset g^{-1}(\beta_\mathcal{S}^{(i)})$, or, $g^{-1}(\beta_\mathcal{S}^{(i)})$ is an open set. As a result, there exists a bijective continuous open map from $\mathcal{S}$ to $\mathcal{V}$, and hence the homeomorphism. $\qquad\square$

## 3    DIG: Topology and Construction

Given a seed voxel $s \in N(S, \xi)$ and a positive integer $\tau$, we define a *discrete iso-contour geodesic* (DIG) as the 0-minimal path whose each voxel $v$ has an intersection with $S$ and a geodesic distance $\tau$ from $s$. We denote this DIG by $\Pi(S, \xi, s, \tau)$. The geodesic distance $d_g(s, v)$ from $s$ to $v$ is given by the length $n$ of the shortest 0-path $\langle v_i : (0 \leqslant i \leqslant n) \wedge v_i \in K(S, \xi) \rangle$ from $s := v_0$ to $v := v_n$, $K(S, \xi)$ being the supercover of $S$.

If a DIG is made of voxels only from the naive voxelization, then it may not be 0-minimal. However, on replacing some of its voxel pairs by some special voxels from the *graceful triangles* corresponding to $S$, it becomes 0-minimal. In analogy with other geometric problems, we term these special voxels as *Steiner voxels*, since they are added to the naive set to make it graceful. Detailed study and analysis related to graceful planes may be seen in [4,5]. As shown in [4], a graceful plane is the thinnest possible voxelized plane on which primitives like lines, triangles, and arbitrary polygons are always connected sets of voxels. Here we show its usefulness for construction of DIG as well.

Let $t$ be a 2-manifold in $S$ with its functional plane $F(t)$, and let $N(t, \xi)$ and $G(t, \xi)$ be the respective naive and graceful planes. Let $p$ and $q$ be two distinct voxels in $N(t, \xi)$, and $p'$ and $q'$ be their respective projections on $F(t)$. Then $p' \neq q'$, due to the one-to-one correspondence between $N(t, \xi)$ and its projection on $F(t)$. Further, if $p$ and $q$ are 0-adjacent (resp., 1- or 2-adjacent) to each other, then $p'$ and $q'$ are also 0-adjacent (resp., 1-adjacent). However, 0-adjacency of $p'$ and $q'$ does not ascertain the connectedness of $p$ and $q$ in $N(t, \xi)$—a typical topological characteristic of naive plane that arises due to *jump* [4]. Figure 2 shows two jump configurations for each functional plane (FP). This is resolved in $G(t, \xi)$ by inserting a Steiner voxel in between the two voxels forming a jump in $N(t, \xi)$ so that the two voxels corresponding to two 0-adjacent pixels on the FP are 0-adjacent in $G(t, \xi)$ as well. The Steiner voxel is chosen from the supercover $K(t, \xi)$ and hence has an intersection with $t$. Observe that the *tandem* formed by the Steiner voxel and its 2-adjacent jump voxel maps to a single pixel on the FP.



FP =    $zx$        $zx$        $xy$        $xy$        $yz$        $yz$
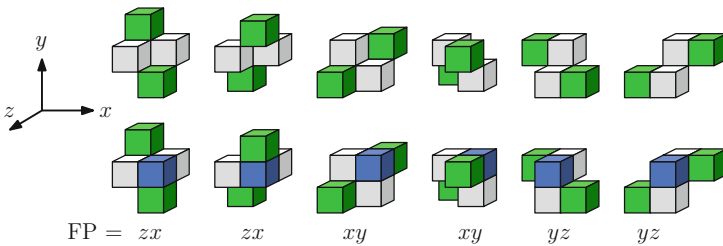
**Fig. 2.** Examples of adding a *Steiner voxel* to a *naive triangle*. **Top:** A *jump* (green voxel pair) on a naive triangle along with its two common 1-adjacent voxels (white). **Bottom:** A *tandem* made by a jump voxel and a *Steiner voxel* (blue) added from the *graceful triangle*. (Color figure online)

We have the following lemma.

**Lemma 1 (Path Projection).** *Let $t$ be a 2-manifold in $S$, and $P$ be a 0-path in $N(t, \xi)$. Then the projection of $P$ on $F(t)$ is 0-minimal if and only if no voxel of $P$ forms a tandem with some voxel in $G(t, \xi)$.*

*Proof.* Let $p, q, r$ be three consecutive voxels in $P$, and $p', q', r'$ be the respective pixels in the projection $P'$ of $P$ on $F(t)$. Clearly, $p', q', r'$ are three distinct pixels on $F(t)$, since $P \subset N(t, \xi)$ and $N(t, \xi)$ has one-to-one correspondence with its projection on $F(t)$. So, $q$ does not make any tandem with $p$ or $r$ in $G(t, \xi)$. Hence, $p'$ and $r'$ are adjacent if and only if $q'$ is simple in $P'$, or equivalently, $q$ forms a tandem with some Steiner voxel in $G(t, \xi)$.                             □

An example of obtaining a 0-minimal path based on Lemma 1 is shown in Fig. 3. Notice that here the path is basically a DIG. By Lemma 1, if the projection $P'$ of $P$ is not 0-minimal in $F(t)$, then there are one or more tandems. Each such tandem is formed by pairing a voxel $q \in N(S, \xi)$ with a voxel $u \in G(S, \xi) \setminus N(S, \xi)$. These local repairs in the constitution of $P$ result in the desired 0-minimality of $P'$ without breaking the connectedness of $P$ in the voxel topology. In particular, we have the following lemma.
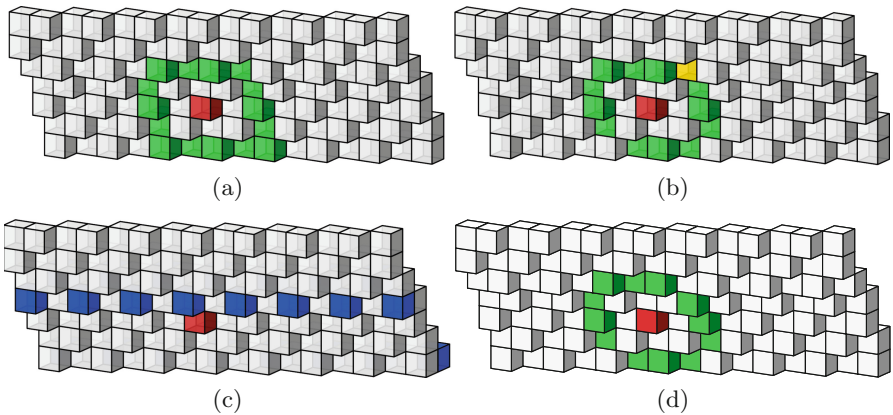


**Fig. 3.** An example showing DIG construction with the seed voxel $s$ shown in red. (a) Green voxels are at geodesic distance 2 from $s$. (b) Back projection (green voxels and one yellow voxel) to the naive plane from the 0-minimal path on the functional plane; the two green voxels adjacent to the yellow voxel form the jump. (c) Graceful plane with the Steiner voxels shown in blue. (d) DIG (green voxels) after replacing one of the jump voxels by a Steiner voxel. (Color figure online)

**Lemma 2 (Steiner Repair).** *Let $P$ be a 0-path in $N(t, \xi)$, $P'$ be its projection on $F(t)$, and $q'$ be the projection of $q \in P$. If $q'$ is a simple pixel, then $q$ and one of its adjacent voxels can be replaced by a single Steiner voxel to ensure the 0-minimality in both $P$ and $P'$.*

*Proof.* As $q'$ is a simple pixel, its preceding pixel $p'$ and succeeding pixel $r'$ in $P'$ are 0-adjacent. Hence, by Lemma 1, one of their pre-images ($p$ or $r$) forms a tandem with some Steiner voxel $u \in G(t, \xi)$. Let, w.l.o.g., that tandem be $(p, u)$. Then replacing $(p, q)$ by $u$ ensures the local minimality in both $P$ and $P'$.  □

We now introduce the following lemma for the theorem that explains the construction of DIG using $N(S, \xi)$ and the Steiner voxels as needed.

**Lemma 3 (Geodesic Distance).** *For any 2-manifold $t$ in $S$, the geodesic distance between two voxels in $N(t, \xi)$ is given by the isothetic distance between their projections on $F(t)$.*

*Proof.* $N(t, \xi)$ has one-to-one correspondence with its projection on $F(t)$. Hence, by definitions of isothetic distance and geodesic distance, the proof follows.  □

Let $B(S, \xi, s, \tau)$ denote the set of voxels from $N(S, \xi)$ having geodesic distance $\tau$ from $s$. This is obtained by breadth-first-search in $N(S, \xi)$ with $s$ as the start vertex in the underlying graph. Let $B(S, \xi, s, \tau)'$ denote the collection of its piecewise projections on the respective functional planes of the participating 2-manifolds of $S$. Let $\Pi(S, \xi, s, \tau)'$ denote the piecewise projections of $\Pi(S, \xi, s, \tau)$ in a similar manner. We have now the following theorem.

**Theorem 2 (DIG).** $\Pi(S, \xi, s, \tau)'$ *is contained in* $B(S, \xi, s, \tau)'$ *and is 0-minimal on the respective functional planes.*

*Proof.* Let $t$ be any 2-manifold in $S$. Let $\Pi_t(S, \xi, s, \tau)$ be the portion of $\Pi(S, \xi, s, \tau)$ corresponding to $t$. Also, let $\Pi_t(S, \xi, s, \tau)' (\subseteq \Pi(S, \xi, s, \tau)')$ be the piecewise projection of $\Pi_t(S, \xi, s, \tau)$ on $F(t)$. Each voxel $q \in \Pi_t(S, \xi, s, \tau)$ has the geodesic distance $d_g(s, q) = \tau$ from $s$. We have two possible cases: either $s$ belongs to $N(t, \xi)$ or it belongs to the naive set of some other 2-manifold in $S$. For the former, $d_g(s, q) = d_\infty(p, q)$ by Lemma 3. For the latter, let $p$ be the voxel lying on a/the geodesic path from $s$ to $q$ and common to $N(t, \xi)$ and $N(t_1, \xi)$, where $t_1$ is a 2-manifold incident on one of the three 1-manifolds of $t$. Then, $d_g(s, q) = d_g(s, p) + d_\infty(p, q)$ by Lemma 3. Hence, in either case, if $q$ (along with one of its adjacent voxels) is replaced by a Steiner voxel $u$ (Lemma 2), then for $u$, we have $d_u(s, u) = d_g(s, q)$. This ensures the containment of $\Pi_t(S, \xi, s, \tau)'$ in $B(S, \xi, s, \tau)'$, and hence the result follows.  □

## 4   Concluding Remarks

We have tested the algorithm for DIG construction on the naive voxel sets of different objects at different scales. On examining and analyzing these test results, it becomes evident that a collection of DIG, constructed with regular geodesic distances of $\tau, 2\tau, 3\tau, \ldots$, from a seed point randomly chosen in $N(S, \xi)$, can aid in inferring on interesting geometric and topological features and the complexity of the object. A couple of such empirical observations are presented here.

See Fig. 4, which shows a collection of DIG, with uniformly changing values of $\tau$, constructed on a regular icosahedron made of 20 equilateral triangles. Notice that the DIG for $\tau = 5$ is almost squarish, since it lies in some triangles whose functional planes are same. As the value of $\tau$ increases to $10, 15, \ldots$, the functional planes of the concerned triangles gradually vary, thereby changing the shape of DIG more and more. If the object is more roundish, such as a regular polyhedron with a larger number of faces, a DIG also becomes more regular and symmetric. The position of the seed point does not have any significant role, and neither the orientation of the object $S$, as far as the scale factor $\xi$ is not uncompromisingly small.
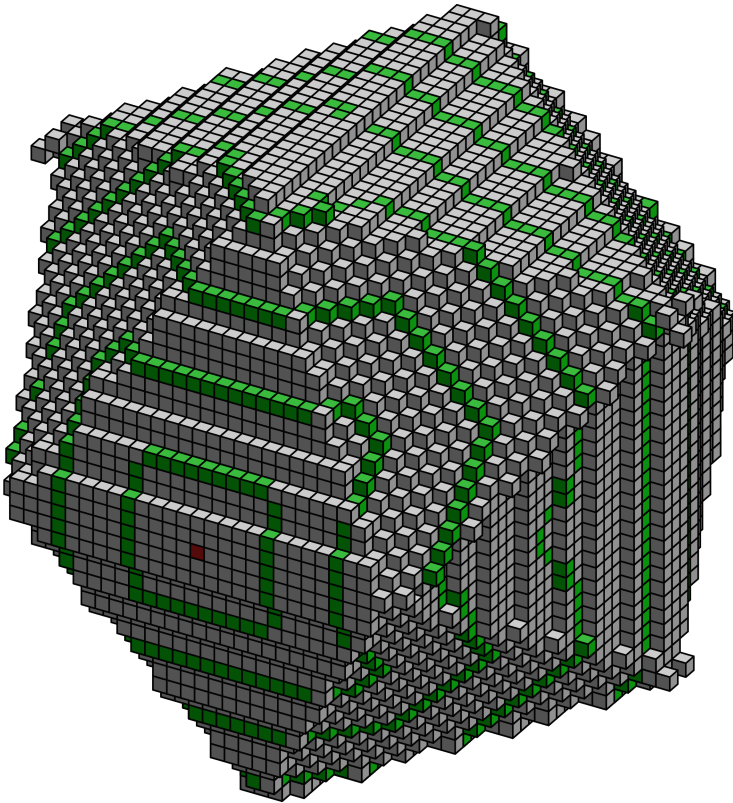


**Fig. 4.** A collection of DIG for $\tau = 5, 10, 15, \ldots$, constructed by our algorithm on the naive set of a regular icosahedron (the seed point $s$ is shown in red). (Color figure online)

The collection of DIG can also be used to detect tunnels in an object, and hence to compute its genus, which is a strong topological feature commonly used for shape analysis. Figure 5 shows a typical set of results on the naive
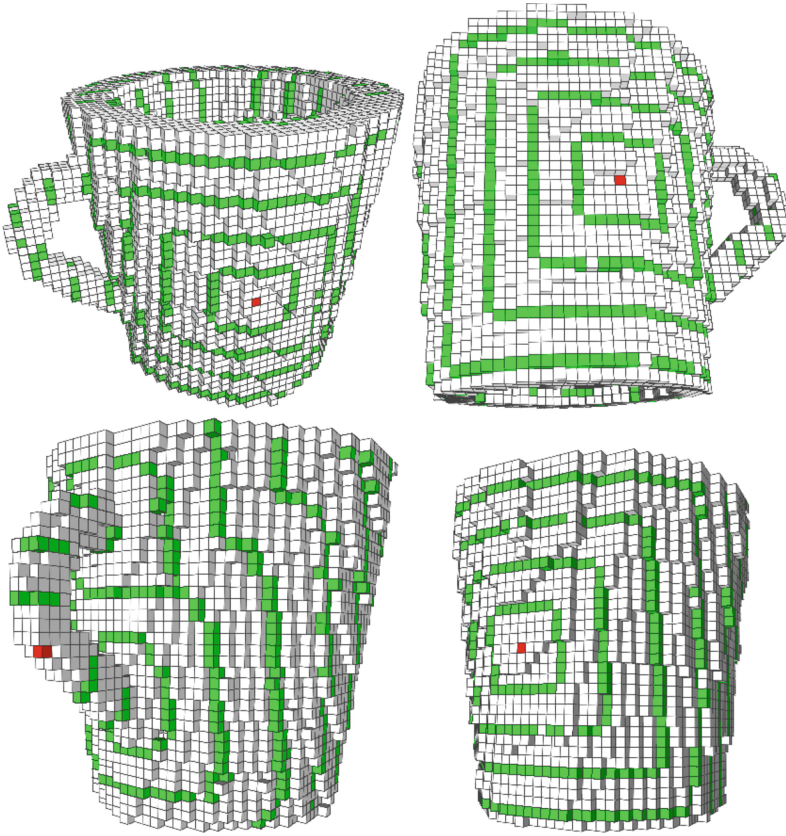
**Fig. 5.** Four collections of DIG (shown in green) on the naive set of a 'mug'. Each collection is generated with a seed point shown in red. (Color figure online)

voxel set of an object with genus one. With four different seed points widely varying in position, the final results in all cases lead to the occurrence of a 'handle' in the object. This is inferred from the fact that in the handle, the DIGs can be paired based on their geodesic distances from $s$. The two DIGs in every pair are geodesically equidistant from $s$, and hence implies two articulation points from the main 'body'. If the two DIGS in the farthest pair among these pairs are connected with each other within a geodesic distance of $2\tau$, then the connecting part belongs to the handle and hence indicates the occurrence of a tunnel; otherwise, it signifies two articulated projections connected through the main body.

The notion of DIG introduced in this paper clearly shows its theoretical merit as well as practical uses in different tasks and applications related to voxelized objects. Setting the value of the scale factor $\xi$ for voxelization of a 2-manifold $S$ in order to ensure its topological equivalence with $S$ through homeomorphism remains an open problem. We foresee this problem important in the theoretical

context of DIG construction and also for shape analysis. Apart from genus and articulation points that are briefly discussed in this paper, many other shape features like regularity, concavity, convexity, and symmetry can also possibly be analyzed through DIG constitution in the voxel space, which if done, would further establish its potential in digital geometry and topology.

# References

1. Balasubramanian, M., Polimeni, J.R., Schwartz, E.L.: Exact geodesics and shortest paths on polyhedral surfaces. IEEE TPAMI **31**, 1006–1016 (2009)
2. Biswas, R., Bhowmick, P.: On different topological classes of spherical geodesic paths and circles in $\mathbb{Z}^3$. Theoret. Comput. Sci. **605**, 146–163 (2015)
3. Brimkov, V.E.: Formulas for the number of $(n-2)$-gaps of binary objects in arbitrary dimension. Discrete Appl. Math. **157**, 452–463 (2009)
4. Brimkov, V.E., Barneva, R.P.: Graceful planes and lines. Theoret. Comput. Sci. **283**, 151–170 (2002)
5. Brimkov, V.E., Coeurjolly, D., Klette, R.: Digital planarity–a review. Discrete Appl. Math. **155**, 468–495 (2007)
6. Chandru, V., Manohar, S., Prakash, C.E.: Voxel-based modeling for layered manufacturing. IEEE Comput. Graph. App. **15**, 42–47 (1995)
7. Chang, H.H., Lai, Y.C., Yao, C.Y., Hua, K.L., Niu, Y., Liu, F.: Geometry-shader-based real-time voxelization and applications. Vis. Comput. **30**, 327–340 (2014)
8. Coeurjolly, D., Miguet, S., Tougne, L.: 2D and 3D visibility in discrete geometry: an application to discrete geodesic paths. PRL **25**, 561–570 (2004)
9. Cohen-Or, D., Kaufman, A.: Fundamentals of surface voxelization. Graph. Models Image Process. **57**, 453–461 (1995)
10. Dachille, F., Kaufman, A.E.: Incremental triangle voxelization. In: Graphics Interface Conference, pp. 205–212 (2000)
11. Desimone, J.M., Ermoshkin, A., Samulski, E.T.: Method and apparatus for three-dimensional fabrication. US Patent 20140361463 (2014)
12. Dionne, O., de Lasa, M.: Geodesic binding for degenerate character geometry using sparse voxelization. IEEE TVCG **20**, 1367–1378 (2014)
13. Dong, Z., Chen, W., Bao, H., Zhang, H., Peng, Q.: Real-time voxelization for complex polygonal models. In: PG 2004, pp. 43–50 (2004)
14. Edelsbrunner, H., Harer, J.L.: Computational Topology. American Mathematical Society, Providence (2009)
15. Eisemann, E., Décoret, X.: Single-pass GPU solid voxelization for real-time applications. In: GI 2008, pp. 73–80 (2008)
16. Fang, S., Fang, S., Chen, H., Chen, H.: Hardware accelerated voxelization. Comput. Graph. **24**, 433–442 (2000)
17. Hiller, J., Lipson, H.: Design and analysis of digital materials for physical 3D voxel printing. Rapid Prototyping J. **15**, 137–149 (2009)
18. Hiller, J., Lipson, H.: Tunable digital material properties for 3D voxel printers. Rapid Prototyping J. **16**, 241–247 (2010)
19. Hull, C.: Apparatus for production of three-dimensional objects by stereolithography. US Patent 4575330 (1986)
20. Jee, H.J., Sachs, E.: A visual simulation technique for 3D printing. Adv. Eng. Softw. **31**, 97–106 (2000)

21. Kamrani, A.K., Nasr, E.A.: Engineering Design and Rapid Prototyping. Springer, Boston (2009)
22. Karabassi, E.A., Papaioannou, G., Theoharis, T.: A fast depth-buffer-based voxelization algorithm. J. Graph. Tools **4**(4), 5–10 (1999)
23. Klette, R., Rosenfeld, A.: Digital Geometry: Geometric Methods for Digital Picture Analysis. Morgan Kaufmann, San Francisco (2004)
24. Liao, D.: GPU-accelerated multi-valued solid voxelization by slice functions in real time. In: VRCAI 2008, pp. 18:1–18:6 (2008)
25. Malgouyres, R.: A discrete radiosity method. In: Braquelaire, A., Lachaud, J.-O., Vialard, A. (eds.) DGCI 2002. LNCS, vol. 2301, p. 428. Springer, Heidelberg (2002)
26. Mitchell, J.S.B., Mount, D.M., Papadimitriou, C.H.: The discrete geodesic problem. SIAM J. Comput. **16**, 647–668 (1987)
27. Mukhopadhyay, J., Das, P.P., Chattopadhyay, S., Bhowmick, P., Chatterji, B.N.: Digital Geometry in Image Processing. CRC, Boca Ration (2013)
28. Nanya, T., Yoshihara, H., Maekawa, T.: Reconstruction of complete 3D models by voxel integration. J. Adv. Mech. Des. Syst. Manuf. **7**, 362–376 (2013)
29. Nooruddin, F.S., Turk, G.: Simplification and repair of polygonal models using volumetric techniques. IEEE TVCG **9**, 191–205 (2003)
30. Pomerantz, I., Cohen-Sabban, J., Bieber, A., Kamir, J., Katz, M., Nagler, M.: Three dimensional modelling apparatus. US Patent 4961154 (1990)
31. Prakash, C., Manohar, S.: Volume rendering of unstructured grids–a voxelization approach. Comput. Graph. **19**, 711–726 (1995)
32. Steingart, Robert, C., Tzu-Wei, D.: Fabrication of non-homogeneous articles via additive manufacturing using three-dimensional voxel-based models. US Patent 8509933 (2013)
33. Surazhsky, V., Surazhsky, T., Kirsanov, D., Gortler, S.J., Hoppe, H.: Fast exact and approximate geodesics on meshes. ACM TOG **24**, 553–560 (2005)
34. Truong-Hong, L., Laefer, D.F., Hinks, T., Carr, H.: Combining an angle criterion with voxelization and the flying voxel method in reconstructing building models from lidar data. Comput. Aided Civ. Infrastruct. Eng. **28**, 112–129 (2013)
35. Xin, S.Q., Wang, G.J.: Improving Chen and Han's algorithm on the discrete geodesic problem. ACM TOG **28**, 104:1–104:8 (2009)
36. Xin, S.Q., Ying, X., He, Y.: Constant-time all-pairs geodesic distance query on triangle meshes. In: I3D 2012, pp. 31–38 (2012)
37. Ying, X., Wang, X., He, Y.: Saddle vertex graph (SVG): a novel solution to the discrete geodesic problem. ACM TOG **32**, 170:1–170:12 (2013)
38. Zhang, Z., Morishima, S.: Application friendly voxelization on GPU by geometry splitting. In: Christie, M., Li, T.-Y. (eds.) SG 2014. LNCS, vol. 8698, pp. 112–120. Springer, Heidelberg (2014)